Model ABC Triblock Copolymers and Blends near the Order−Disorder Transition

Cordell M. Hardy and Frank S. Bates*

Department of Chemical Engineering and Materials Science, University of Minnesota, Minneapolis, Minnesota 55455

Man-Ho Kim and George D. Wignall

Oak Ridge National Laboratory, P.O. Box 2008 MS6393, Oak Ridge, Tennessee 37831

Received August 29, 2001

ABSTRACT: We report differences in the thermodynamic behavior of compositionally symmetric ABC and BAC triblock copolymers near the order−disorder transition temperature and of binary ABC/BAC copolymer blends: poly(styrene-*b*-isoprene-*b*-dimethylsiloxane) (SID) and ISD with segment volume fractions near 0.33 and similar molecular weight disorder at different temperatures and from different ordered-state symmetries. Blends of symmetric SID and ISD molecules with molecular weights near 10K are miscible and form a gyroid morphology over a wide range of blend compositions. Flory−Huggins interaction parameters for this ABC system allow a detailed interpretation of SAXS, SANS, and DMS measurements. Symmetric SID disorders from the lamellar state, while ISD disorders from hexagonally packed cylinders of D blocks in a mixed matrix of S and I blocks. Block mixing occurs to reduce the number of S−D interactions forced by chemical connectivity in ISD. This drive to minimize unfavorable interactions is the underlying cause of the results outlined in this report.

I. Introduction

Block copolymers, which have captured the imagination of polymer scientists and engineers for over 40 years, now account for important segments of the plastics and rubber industries.[1] Conventional applications rely on ABA type triblock copolymers, usually based on polystyrene and polydiene blocks. Experimental[2] and theoretical[3,4] research have provided a rather comprehensive description of the phase behavior of this and other linear two-monomer (AB, ABABA, etc.) block copolymers, including universal phase diagrams[3] that incorporate the experimentally accessible parameters of molecular weight (or degree of polymerization N) and composition. The choice of monomers and the environmental conditions (temperature and pressure) establish the magnitude of the segment−segment interaction parameter χ. For AB diblock and ABA triblock copolymers four ordered equilibrium morphologies are now well established: lamellae, gyroid, cylinders, and spheres. It is unlikely that additional nanostructures will be added to this list. Beginning in the 1980s, with the seminal work of Matsushita and co-workers,[5,6] followed by the expansive and illuminating studies by Stadler and co-workers[7−10] and others,[11] it has become apparent that a seemingly unlimited array of ordered block copolymer phases can be accessed by adding additional chemically distinct blocks to the traditional two-monomer pallet in linear[12] and branched[13] configurations. This presents a daunting challenge to the practitioner interested in designing a specific morphology. In this article we restrict our attention to the simplest case, linear ABC triblock copolymers.

Most prior experimental studies dealing with ABC triblock copolymers have focused on relatively strongly segregated blocks. Dozens of fascinating morphologies have been reported, including various combinations of the traditional nanostructures (e.g., spheres between lamellae, cylinders between lamellae, and rings on cylinders, etc.[8,14]) and several unusual complex geometries like the knitting pattern[15] and the core−shell gyroid.[11] This wealth of structures is not unanticipated[12] since the number of parameters that must be balanced, and the degrees of freedom in designing these molecules, is significantly greater than for the well-characterized two-monomer cases. Three different blocks imply two independent composition variables, three separate χ parameters, and three different block sequences. While the fundamental principles for phase selection in ABC's are essentially identical to those governing AB's (e.g., minimization of interfacial area and chain distortion[16]), the expanded number of possible structures seriously complicates application of conventional theoretical approaches such as self-consistent-field theory (SCFT),[17] where the ordered state symmetry is a starting condition. Moreover, segregation strengths often are distributed asymmetrically, resulting in considerably stronger segregation between two of the blocks. For example, when $\chi_{AB} \ll \chi_{BC} \approx \chi_{AC}$ in an ABC triblock, the B and C and A and C blocks will segregate strongly while intermediate or weak segregation will exist between A and B. For high-symmetry structures like the core−shell gyroid[11] this further complicates mean-field SCFT calculations.

Recently, Drolet and Fredrickson[18] have proposed a new approach to predicting block copolymer phase behavior, one that does not rely on a priori knowledge of the equilibrium phase symmetry and in principle is not hampered by strong segregation. This represents a revolutionary breakthrough, which promises to provide guidance in the quest to produce real materials endowed with multiple properties derived from multiple polymer blocks. Based on our experience with two-monomer block copolymers,[19] the region of phase space around the order−disorder transition (ODT) represents the most reliable place to obtain equilibrium phase behavior data for comparison with theory. Moreover, most ap-

10.1021/ma0115489 CCC: $22.00
Published on Web 03/09/2002

plications require processing which is often done in the disordered state. With this in mind we have developed several model ABC block copolymer systems that can be placed near the ODT for basic thermodynamic studies. This article deals with one of these, constructed from styrene (S), isoprene (I), and dimethylsiloxane (D) repeat units.

Previous studies have shown that poly(isoprene-*b*-styrene-*b*-dimethylsiloxane) (ISD)[11] and SID[20] block copolymers can display interesting and potentially useful phase behavior and properties. These polymers can be synthesized in relatively large quantities (ca. 0.1 kg batches) in nearly monodisperse form using anionic polymerization techniques.[21] In addition, the magnitudes of χ_{SI}, χ_{ID}, and χ_{SD}[11,22] should place the disordering temperature within a tractable experimental window ($100 < T < 250$ °C) at modest molecular weights (ca. 10^4 g/mol); this is an important consideration due to the harsh kinetic penalties encountered while pursuing equilibrium phase behavior at higher molecular weights.[23,24] Another advantage is our ability to prepare complementary ISD and SID specimens for use in examining the consequences of block sequence variation. This publication describes the phase behavior of several ISD and SID triblocks that access the disordered state. A combination of small-angle X-ray and neutron scattering (SAXS and SANS) and dynamic mechanical spectroscopy (DMS) have been employed to establish ordered state symmetries, T_{ODT}'s, and the nature of the disordered melts. Well-defined complementary specimens allow us to draw quantitative conclusions regarding the role of sequencing near the ODT.

Sequence differences introduce another fascinating feature to ABC block copolymers.[25,26] Blending AB diblocks is a convenient way to create intermediate morphologies such as the gyroid without an extensive investment in polymer synthesis.[27] Blending SID and ISD, with comparable molecular weights and compositions, creates a new type of chain packing frustration, with the potential for macroscopic phase separation or new homogeneous morphologies as reported by Abetz et al.[28] in strongly segregated specimens. We address this problem with the model ISD and SID polymers near the ODT, establishing the phase diagram for complementary triblocks.

This paper is organized as follows. Section II outlines our experimental procedures, followed by the presentation and analysis of the DMS, SAXS, and SANS results in section III. A discussion of our findings and comparison with other studies is dealt with in section IV, and we conclude with a summary in section V.

II. Experimental Section

Synthesis and Characterization. Poly(styrene-*b*-isoprene-*b*-dimethylsiloxane) (SID) and poly(isoprene-*b*-styrene-*b*-dimethylsiloxane) (ISD) triblock copolymers discussed in this report were prepared using anionic polymerization techniques and equipment described elsewhere.[29] The preparation of ISD triblock copolymers is achieved through sequential polymerization of the appropriate monomers and has recently been discussed in some detail by Shefelbine et al.[11]

A typical SID synthesis proceeded as follows: styrene (19.4 g) was initiated using *sec*-butyllithium and allowed to polymerize for 4 h at 40 °C in 212 g of cyclohexane. Isoprene (16.6 g) was then added to the reactor and allowed to react for 4 h, after which the solution was cooled to 25 °C. To add the poly(dimethylsiloxane) block, a 42 wt % solution of hexamethylcyclotrisiloxane (D_3) was prepared in cyclohexane, and 85.1 g of solution was added to the reaction mixture. Because polymerization of the D_3 monomer is very slow in apolar solvents like cyclohexane, addition of 190 g of tetrahydrofuran followed addition of the D_3 solution. This stimulated rapid initiation of D_3 and provided a polar medium for polymerization. After 4 h, the time estimated for 50% D_3 conversion,[30] the reaction was terminated using excess trimethylchlorosilane.

The product was recovered by reduction of the solution volume to approximately one-half the original amount by evaporation, followed by precipitation into methanol. The polymer was washed with methanol and dissolved in THF. A small amount of 2,6-di-*tert*-butyl-4-methylphenol antioxidant (~0.3 wt %) was added, and the purified polymer was dried to constant weight at 70 °C under vacuum. Typical polymerizations of ISD triblock copolymers proceeded as above, with the order of styrene and isoprene addition reversed.

^{1}H NMR (Varian-500 MHz) spectra obtained from deuterated chloroform solutions containing 10 mg/mL polymer were used to determine the triblock copolymer weight compositions. Volume fractions are calculated on the basis of the published homopolymer densities at 140 °C for each block ($\rho_S = 0.969$ g/cm^3, $\rho_I = 0.830$ g/cm^3, $\rho_D = 0.895$ g/cm^3).[31]

A combination of NMR and gel permeation chromatography (GPC) was used to determine the overall molecular weight of each polymer. An aliquot of the first living block was taken (S or I), quenched in methanol, and analyzed using GPC. For I blocks, Mark−Houwink constants were used to relate polyisoprene elution volumes to a calibration curve based on polystyrene standards. The molecular weight of the first block was then used with the NMR-determined segment weight fractions in the complete triblock to determine the overall molecular weight. These results compare favorably with the molecular weights estimated through end-group analysis by ^{1}H NMR alone as well as the molecular weights estimated from reaction stoichiometries.

GPC was used to establish the overall polydispersity of each copolymer relative to polystyrene standards and to determine the amount of homopolymer and/or diblock copolymer impurities.

Blends of SID and ISD triblock copolymers, discussed below, were prepared by solvent-casting from tetrahydrofuran. Blends throughout the composition range were dried at 70 °C under vacuum to constant weight.

Small-Angle X-ray Scattering. SAXS experiments were conducted on a small-angle beamline operated at the University of Minnesota. Cu Kα X-rays were generated by a Rigaku RU-200BVH rotating anode and an X-ray machine equipped with a 0.2 × 2 mm microfocus cathode and Franks mirror optics. Samples were placed inside an evacuated sample chamber and maintained at the desired temperatures by a pair of heaters mounted on a water-cooled brass block. The temperature range was 45−210 °C (±0.1 °C). Two-dimensional diffraction images were collected with a multiwire area detector (HI-STAR, Siemens Analytical X-ray Instruments) and corrected for detector response characteristics and background scattering prior to analysis. Azimuthal integration of the 2-D data produced plots of intensity I vs scattering wave vector magnitude $q = 4\pi\lambda^{-1}\sin(\theta/2)$, where λ and θ are the radiation wavelength (1.54 Å) and scattering angle, respectively.

Small-Angle Neutron Scattering. The initial SANS experiments were performed on the KWS1 SANS facility[32] at the FRJ2 research reactor in Jülich, with a wavelength of $\lambda = 7$ Å ($\Delta\lambda/\lambda = 0.20$) and later complemented by measurements at the National Institute for Standards and Technology (NIST) in Gaithersburg, using $\lambda = 6$ Å ($\Delta\lambda/\lambda = 0.10$). Measurements were undertaken with the same sample−detector distance (4 m) on both instruments; the smaller wavelength range of the latter facility minimizes instrumental "smearing" effects,[33] to which the "peaks" observed in this study are particularly sensitive. Most intersample comparisons were therefore made on the NIST instrument, though for a given sample run on both facilities (e.g., ISD1), the same ODT was observed within an error of ±1.5 °C, and this serves as a useful cross-calibration. All data sets were corrected for instrumental sensitivity as described previously[33] and normalized to an

Table 1. Triblock Characterization Data

sample	$10^3 M_n$[a]	M_w/M_n[b]	f_S[c]	f_I[c]	f_D[c]	T_{ODT} (°C)[d]
ISD1	9.4	1.14	0.343	0.341	0.316	117
ISD2	31	1.09	0.374	0.342	0.284	> 240
ISD4	12.3	1.06	0.378	0.360	0.262	165
SID7	8.5	1.14	0.331	0.322	0.347	227
SID8	7.5	1.18	0.297	0.320	0.383	127

[a] Determined by GPC, in units of g/mol. [b] Based on polystyrene standards. [c] Volume fractions of repeat units as determined by NMR and published densities (see Experimental Section). Our estimate of uncertainty in volume composition is ±2 vol %. [d] Measured by DMS.

absolute (±4%) differential cross section per unit sample volume [$d\Sigma/d\Omega(Q)$ in units of cm^{-1}] by the same precalibrated secondary standards.

Dynamic Mechanical Spectroscopy (DMS). DMS is useful for determining approximate temperatures at which block copolymers undergo order−order and order−disorder transitions (OOTs and ODTs).[34] Constant-frequency (1 rad/s) temperature measurements using either a Rheometrics ARES strain-controlled rheometer or a Rheometrics DSR stress-controlled rheometer were conducted while increasing the temperature to measure the dynamic elastic modulus (G') at 1 °C/min. Discontinuous, large decreases in G' with heating indicate the loss of ordering through a first-order transition into the disordered state. Samples were 0.7−1.1 mm thick, and the parallel plates used were 25 mm in diameter. A nitrogen purge was employed to minimize oxidative degradation at elevated temperatures. Strains were kept to between 1 and 5% for these samples, within the linear viscoelastic regime. It was necessary to use strains of at least 1% to ensure that meaningful stresses were generated on the instrument and to gradually increase the strain with heating as the modulus decreased. DMS also was used to estimate the glass transition temperature for poly(styrene). In all cases the experimental data presented here were obtained above T_g.

III. Results and Analysis

In this section we present the experimental results obtained from the neat SID and ISD triblock copolymers and a series of binary SID/ISD blends. DMS, SAXS, and SANS results are reported and evaluated in two parts and then discussed in section IV. Here we note that attempts to characterize the triblock morphologies, particularly near the ODT, by transmission electron microscopy were largely unsuccessful as a consequence of the soft material properties and temperature-dependent symmetry of the most critical samples.

SID and ISD Triblocks. Dynamic mechanical spectroscopy data were obtained as a function of temperature at a constant frequency ($\omega = 1$ rad/s) for the five triblock copolymers listed in Table 1. Dynamic elastic shear modulus, $G'(T)$, data are presented in Figure 1. In each case the modulus decreases monotonically with increasing temperature, and in four of the five materials G' drops precipitously at specific temperatures identified by arrows and listed in Table 1. Experience with numerous block copolymers[35,36] leads us to associate this abrupt loss of elasticity with the order−disorder transition temperature (T_{ODT}). One sample, ISD2, retained a relatively elastic response over the entire experimental temperature range, suggesting that $T_{ODT} > 240$ °C. The rise in G' between 60 and 75 °C for ISD4 indicates a thermally induced change in microstructure, but the featureless viscoelastic behavior for $T < T_{ODT}$ suggests that no order−order transitions occur in the other samples. A striking feature associated with these results is the 110 °C difference in T_{ODT} between ISD1 and SID7, samples with essentially identical compositions and molecular weights.

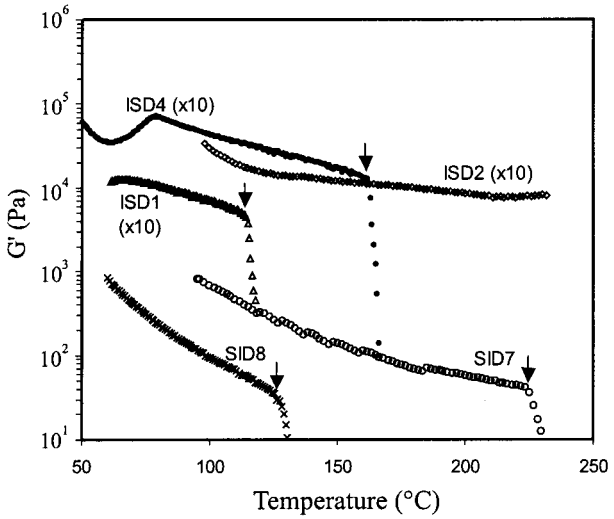

Figure 1. DMS results for all five samples considered in this report. Samples were heated at 1 °C/min, $\omega = 1$ rad/s. ISD1, SID8, ISD4, and SID7 show ODT temperatures at 117, 127, 165, and 227 °C, respectively, as indicated by the arrows. ISD2, having a molecular weight substantially higher than the other three polymers, did not show a disordering transition below 240 °C. The increase in G' between 60 and 75 °C for ISD4 is interpreted as an order−order transition.

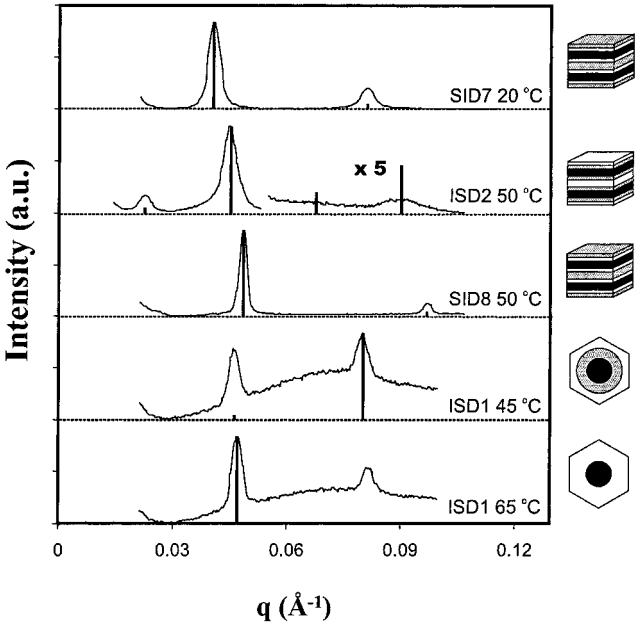

Figure 2. Representative ordered-state SAXS patterns. Each set of data was collected from azimuthally integrated 2-D plots. The solid vertical lines presented with each trace represent relative peak intensity calculations discussed in the Appendix. Electron density profiles were approximated using homopolymer mass densities for each block and the corresponding idealized morphology schematically illustrated at the right of each data series. Data for ISD1 are presented at two temperatures to contrast the results of calculations for core−shell and homogeneous cylindrical morphologies with the temperature-dependent relative peak intensities of ordered ISD1.

Small-angle X-ray scattering patterns were recorded for each triblock copolymer at various temperatures, and representative examples are shown in Figure 2. (SAXS data for ISD4 are shown separately in Figure 6.) Each of these scattering patterns contains two or more relatively sharp peaks indicative of an ordered structure. Those from samples ISD2, SID7, and SID8 are characterized by the sequence q^*, $2q^*$, $3q^*$, ... where q^*

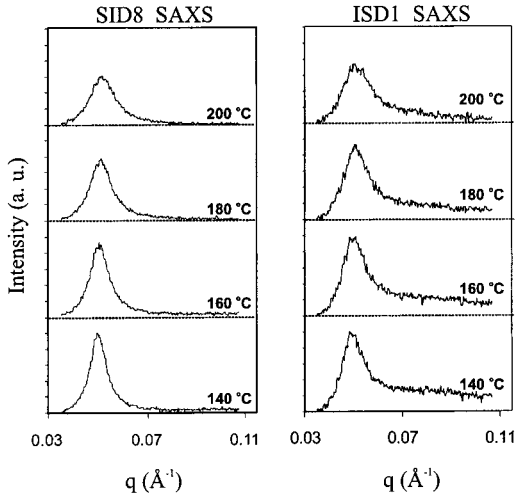

Figure 3. Selected SAXS data for SID8 and ISD1 at temperatures between 140 and 200 °C. There is distinctively high scattering intensity for ISD1 at higher values of q in the disordered state at temperatures slightly higher than T_{ODT}.

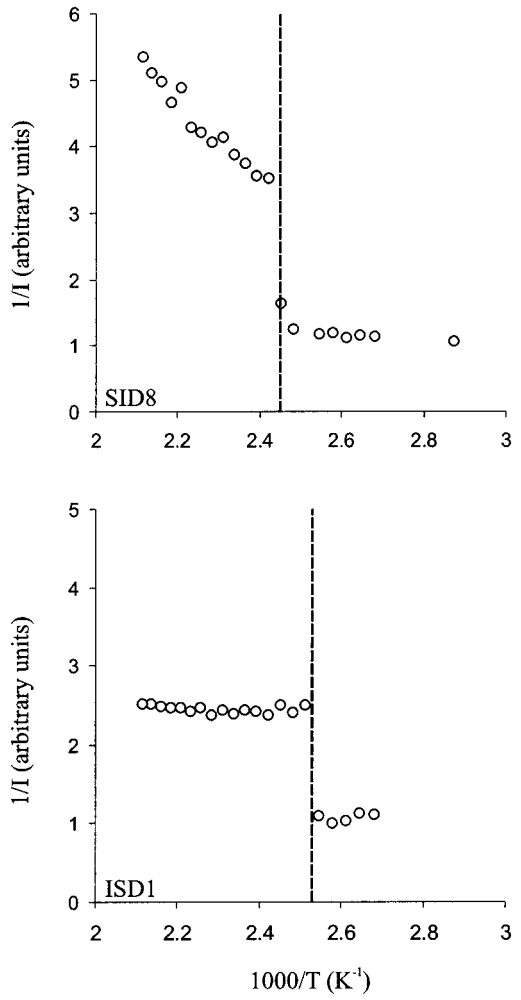

Figure 4. Plots of inverse SAXS peak intensity $1/I(q^*)$ vs inverse temperature. At $1/T_{ODT}$ there is a discontinuity in $1/I(q^*)$. While the maximum scattering intensity in SID8 decreases with increasing temperature in the disordered state, $I(q^*)$ is essentially independent of temperature changes for $T_{ODT} < T < 200$ °C in ISD1.

is the scattering wavevector for the lowest order reflection. This familiar pattern is consistent with a lamellar morphology. Closer examination of these three SAXS traces reveals a distinct difference between the one from

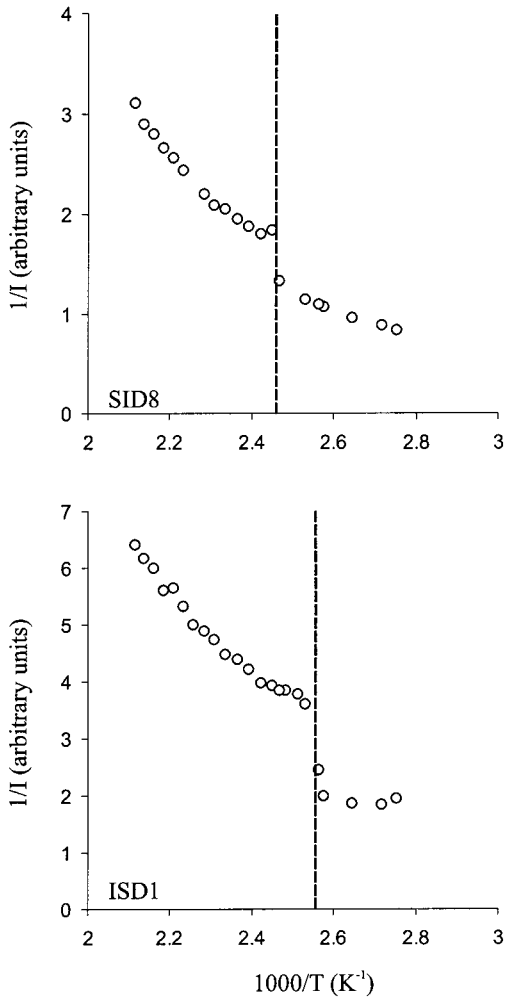

Figure 5. $1/I(q^*)$ vs $1/T$ collected from SANS data. Both ISD1 and SID8 show a decrease in $I(q^*)$ with increasing temperature and T_{ODT} values consistent with the SAXS and DMS results.

ISD2 and those from SID7 and SID8. In the former the first-order reflection occurs at nearly half the q value found in the other two and at a small fraction of the greatest peak intensity. These effects, which did not change significantly with temperature, reflect differences in the lamellar stacking sequences for ISD vs SID. As detailed in the Appendix, shuffling the electron density distribution ($\rho_D > \rho_S > \rho_I$) leads to distinct changes in the diffraction conditions. We have estimated the relative intensities for ideal stacks of pure S, D, and I sheets, constrained by the length scale established by the leading SAXS reflections ($d^* = 2\pi/q^*$) and the block copolymer compositions (Table 1). These results are depicted as vertical lines in Figure 2. These calculations capture the qualitative features in the data, supporting the morphological assignments illustrated by the sketches alongside the SAXS results.

Sample ISD1 behaved differently. First, the two diffraction peaks appear with the ratio q^*, $\sqrt{3}q^*$. Second, the relative intensities of the first- and second-order peaks change with temperature. And third, a broad maximum centered near 0.08 $Å^{-1}$ and ranging from 0.03 $Å^{-1}$ to greater than 0.1 $Å^{-1}$ is convoluted with the diffraction peaks. We have tentatively identified the morphology of ISD1 as hexagonally ordered cylinders based on the relative peak positions found in Figure 2. In a separate experiment (not shown) ISD1 was subjected to an oscillatory shear deformation, then inter-

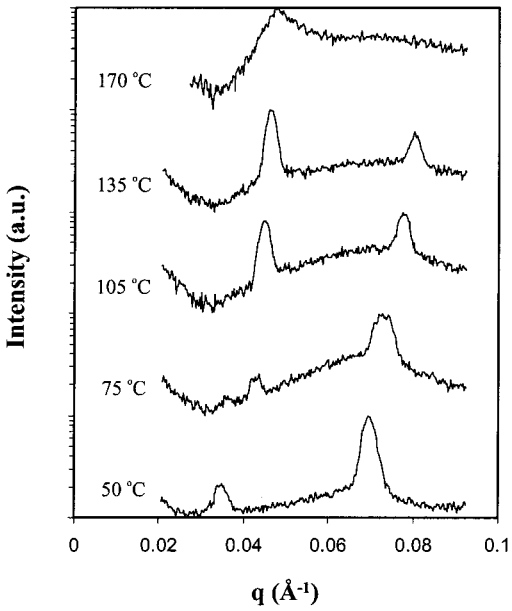

Figure 6. Representative SAXS data for ISD4 obtained at various temperatures. Three phases are associated with these patterns: lamellae (50 °C), cylindrical (75−135 °C), and disordered (170 °C). Development of a broad maximum at 75 °C and higher temperatures is attributed to mixing of S and I blocks which accompanies the three-domain lamellae to two-domain cylinder transition between 50 and 75 °C.

rogated by SAXS, with the beam directed along the axis of shear. Six equally spaced, azimuthally smeared maxima were recorded on the area detector, consistent with our assignment of hexagonal symmetry.

The broad scattering maximum in the ISD1 SAXS patterns is reminiscent of the familiar correlation hole effect in disordered block copolymers.[4] It reflects extensive scattering over a wide range of length scales, suggestive of partial mixing between two of the blocks. On the basis of estimated χ parameters (see Discussion section), we anticipate preferential mixing of the S and I blocks and minimal D interfacial area. Two limiting composition profiles can be imagined: a "three-domain" core (D)−shell (S)−matrix (I) and a "two-domain" core (D)−matrix (S + I) composition profile, each illustrated in Figure 2. Using the strategy outlined in the Appendix, relative SAXS diffraction intensities have been calculated for these two limiting cases as shown by the vertical lines in Figure 2. These calculations capture the qualitative trends exhibited by ISD1 upon heating, i.e., an increase in the intensity of the first-order peak at the expense of the second. On the basis of the intermediate experimental SAXS behavior, we believe ISD1 contains a quasi-two-domain cylindrical morphology with a partially segregated (or graded) S + I matrix.

Samples SID8 and ISD1 also were examined in the disordered states as a function of temperature by SAXS with representative results given in Figure 3. A relatively broad peak characterizes all these data. However, noticeable differences are evident between the SID8 and ISD1 results. ISD1 appears to develop a second broad peak at higher q as the sample is cooled toward T_{ODT}. This effect will be considered in more detail in a separate publication[37] along with additional data from other disordered triblocks containing varying levels of contrast. Here, we focus on the peak intensities, which are plotted as a function of inverse temperature in Figures 4 (SAXS) and 5 (SANS). In all cases the ODT is signaled by a discontinuous drop in peak intensity

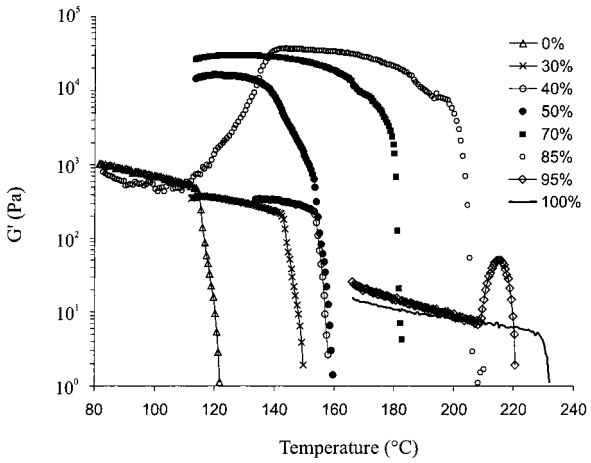

Figure 7. DMS results for blends of SID7 and ISD1 obtained at $\omega = 1$ rad/s. Listed compositions are of weight percent SID7 in ISD1. Indicated by the sharp drop in the dynamic elastic modulus with heating, T_{ODT} varies with blend composition. The high modulus below T_{ODT} for compositions between 50 and 85% is consistent with formation of the gyroid phase.

with heating, at the same temperatures identified by DMS, as commonly reported with diblocks.[34] However, the temperature dependence of $I(q^*)$ is distinctly dependent on radiation type, with the most dramatic example being ISD1 where the peak intensity in the disordered state is essentially independent of temperature.

Representative SAXS data for ISD4 are shown in Figure 6. At temperatures below 50 °C ISD4 displays a pattern characteristic of lamellae with relative peak intensities similar to those of ISD2 (Figure 2, at 50 °C). Upon heating to 75 °C the second-order peak location evolves from $2q^*$ to $\sqrt{3}q^*$. Further heating causes a gradual decrease in the relative intensity of the second-order peak. As discussed above in relation to ISD1, we interpret these changes in relative peak intensities as the result of temperature-dependent mixing of S and I blocks in cylindrical ISD samples.

While we were unable to shear ISD4 sample in situ, alignment of this sample was achieved prior to some SAXS measurements using a rheometer. Shear-aligned samples yielded 2-D SAXS patterns containing smeared spots azimuthally separated by 180° at q^* and $2q^*$, indicative of a lamellar morphology similar to that observed for ISD2. Upon heating through the lamellar-to-cylindrical transition, previously aligned samples showed coaxially located spots at q^* and $\sqrt{3}q^*$. A display of planar orientation and peaks consistent with a hexagonal symmetry strongly suggests the cylindrical morphology assigned to ISD1 and ISD4, although in the absence of in-situ shear we were unable to coerce ISD4 into sufficient alignment for six maxima to appear on the circle $|\mathbf{q}| = q^*$. With heating, ISD4 undergoes a transition from "three-color" lamellae to "two-color" cylinders prior to disordering at 165 °C. Figure 10 illustrates the overall sequence of phases for symmetric SID and ISD.

SID7/ISD1 Blends. We have explored the consequences of blending sequentially distinct triblocks using samples SID7 and ISD1. These homologous polymers contain equal fractions of each block and nearly identical molecular weights. Representative DMS experiments, conducted at $\omega = 1$ rad/s, are presented in Figure 7 where the composition refers to the weight percent of SID7 in ISD1. These G' curves each contain a precipi-

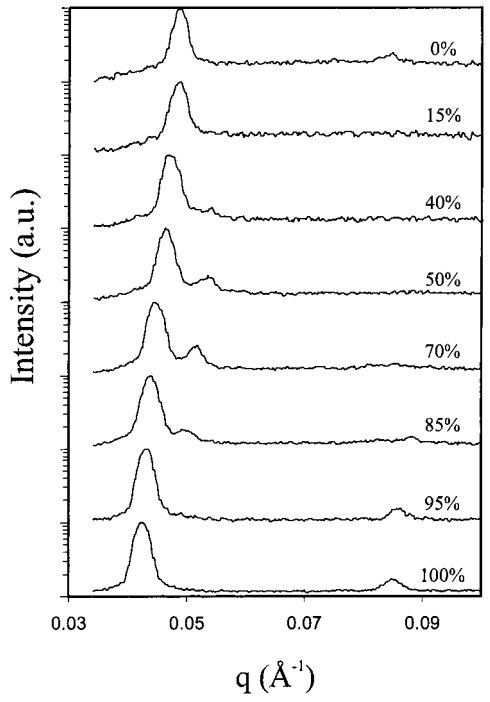

Figure 8. Representative SAXS results for blends of SID7 and ISD1 (compositions specified are wt % SID7, $T = 110$ °C). Increasing composition causes a progression from hexagonally packed cylindrical, to gyroid, to lamellar morphologies.

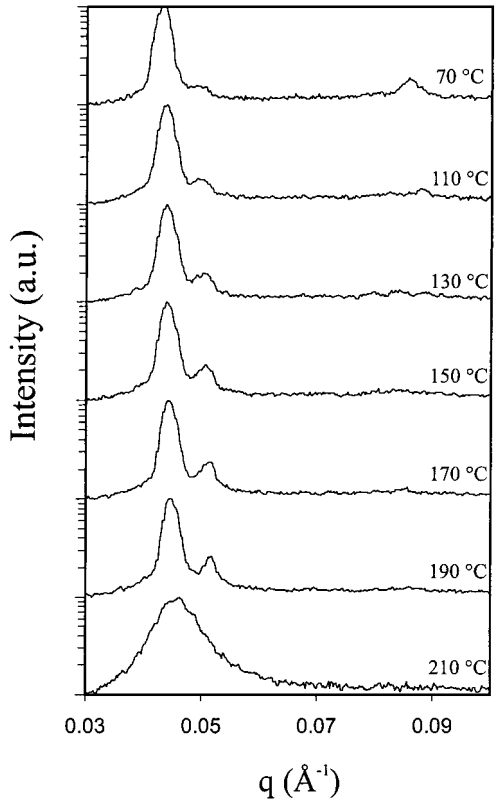

Figure 9. SAXS data for a blend of 85% SID7 in ISD1 for temperatures ranging from 70 to 210 °C. Heating causes an apparent transition from lamellar to gyroid morphologies and then to disorder. Even at the lowest temperature considered here, peaks consistent with both lamellae and the gyroid are evident, although only gyroidlike scattering persists at temperatures above 130 °C.

tous drop at a temperature that we associate with the ODT. (Here we note that the Gibbs phase rule dictates that a two-phase envelope must separate the ordered and disordered phases. Similar to our earlier treatment of diblock blends,[27] we do not attempt to resolve this feature here, although it may be responsible for the intermediate falloff in G' between about 138 and 155 °C for the 50% results.)

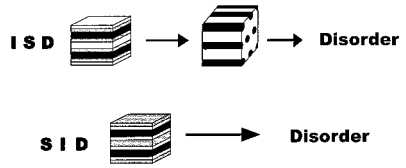

Figure 10. Schematic summary of thermodynamic phase behavior for neat, compositionally symmetric SID and ISD copolymers. Heating ISD or decreasing the molecular weight causes a transition from three-domain lamellae to hexagonally packed two-domain cylindrical morphologies, followed by disordering. SID disorders directly from the three-domain lamellar state.

Other significant transitions in elastic response are evident as the composition increases from 40 to 50% (G' jumps nearly 2 orders of magnitude) and 85 to 95% (a reduction of 3 orders of magnitude). The 85% sample undergoes a transition between roughly 110 and 140 °C, while the 95% blend exhibits a small but distinct increase in G' at 208 °C before plummeting at nearly 220 °C. We associate these changes with order−order transitions (OOT's), much like we and others have done earlier with two-monomer block copolymers[38] and blends.[27] Because these transitions were determined while heating the samples at a finite rate, the true equilibrium T_{OOT} values may be slightly lower.

Insight into the underlying morphologies of these blends can be gleaned from SAXS measurements. Figure 8 contains powder patterns from six blends along with those for the pure components, already identified as hexagonally packed "two-domain" cylinders (ISD1) and "three-domain" lamellae (SID7). Between 40 and 85% SID7 a new scattering pattern appears, one quite familiar to anyone who has worked with the "two-domain" gyroid phase.[39] Two reflections with a relative spacing of $\sqrt{6}q^*$ to $\sqrt{8}q^*$, and corresponding peak intensities of roughly 10 to 1, are the signature of this double network morphology. Three-domain gyroid structures (either $I4_132$ or $Ia\bar{3}d$ space groups) produce qualitatively different scattering patterns.[11] Moreover, these scattering results coincide with a relatively high elastic modulus (see Figure 7), also consistent with a triply periodic phase.[40] At 85% SID7 there appears to be a small higher order reflection at $2q^*$ suggestive of some amount of the lamellar phase. Therefore, this sample was examined as a function of temperature from 70 to 210 °C, and representative SAXS data are shown in Figure 9. Decreasing the temperature to 70 °C increased the magnitude of the $2q^*$ peak at the expense of the $\sqrt{8}q^*$ reflection intensity. We interpret this as exchange of gyroid for lamellar morphology with cooling, consistent with traversing a two-phase window. On the other hand, heating to 130 °C, and subsequently T_{ODT}, eliminates the lamellar component, leaving only a gyroid SAXS signal, which persists until disordering. Our blend results are summarized in the form of a phase diagram in Figure 11.

IV. Discussion

The results presented in the previous section establish the phase behavior of nearly symmetric SID and ISD

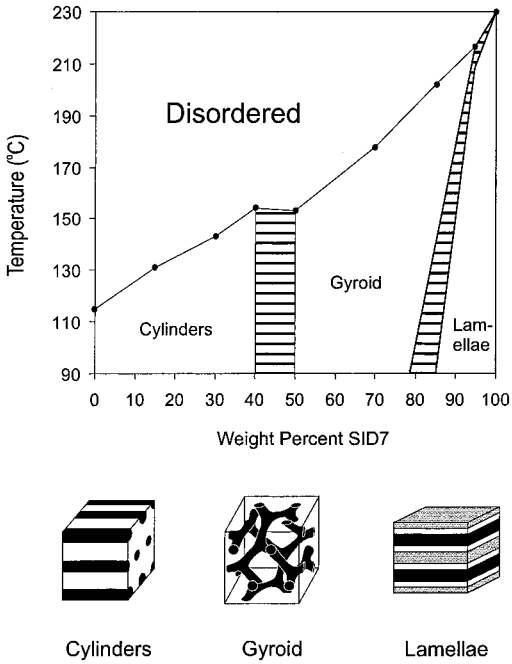

Figure 11. Phase diagram for blends of SID7 and ISD1. Horizontal patterned lines in the plot represent coarsely defined coexistence regions. Increasing the composition of SID7 causes a progression from cylindrical (two-domain), to gyroid (two-domain), to lamellar (three-domain) morphologies. These blend samples exhibit classical alloying behavior throughout the composition range, generally achieving long-range order below T_{ODT} through mixing of S and I blocks.

triblock copolymers, and the associated binary blends, near the order−disorder transition. Perhaps the most striking feature is that all the reported structures were obtained from a single set of compositions, $f_I \approx f_S \approx f_D$. (We ignore the small differences in composition found in Table 1.) Variation in segment sequencing results in qualitatively different routes to disorder and quantitatively different ODT temperatures in the neat materials, which we attribute to frustration effects. Blending ISD and SID provides a new strategy for manipulating the state of order without changing the overall chemical composition. In this section we consider these findings in the context of conventional block copolymer theory. Of central importance to this discussion are the three segment−segment interaction parameters that control the enthalpic contributions to the overall free energy of the ordered and disordered states. These have been estimated on the basis of experimental diblock copolymer phase behavior[11,22] together with mean-field theory,[4]

$$\chi_{SI} = 33.0/T - 0.023$$

$$\chi_{ID} = 43.6/T - 0.010$$

$$\chi_{SD} = 68.0/T - 0.037$$

where the reference volume corresponds to a polystyrene repeat unit. For the entire temperature range covered in this study, $\chi_{SD} > \chi_{ID} > \chi_{SI}$.

Neat Triblock Copolymers. The phase behavior of the two SID and three ISD triblock copolymers can be rationalized on the basis of the three χ parameters listed above. Both SID specimens form three domain lamellae that transform directly to the disordered state upon heating. This microstructural arrangement results in I/S and I/D interfaces, avoiding the least favorable S/D contacts. Increasing molecular weight (from SID8 to SID7) produces a predictable elevation in T_{ODT}.

Inverting the sequence of blocks introduces a frustration condition. In the ISD arrangement D and S blocks are destined to maintain some area of contact. At the strongest degree of segregation, accessed with sample ISD2, a three domain lamellae morphology persists over the entire experimental temperature range. (For a given architecture and composition we associate segregation strength with the overall degree of polymerization by analogy with diblock copolymers.[3]) Obviously, packing constraints and chain stretching contributions overwhelm any enthalpic benefit associated with other morphologies. To characterize the transition from strong to weak segregation while capturing any order−order phase transitions, it was necessary to splice together data from several ISD specimens. ISD4 provided the link between the (three domain) lamellae and (two domain) cylindrical phases, with the order−order transition (OOT) occurring at about 70 °C (see Figures 1 and 6). We interpret this OOT based on the minimization of unfavorable S/D contacts. χ_{SI} is the smallest interaction parameter in this system, and mixing of S and I blocks screens S/D contacts. Upon mixing, the S + I domain acquires a volume fraction of approximately $^2/_3$, a natural composition for the formation of D cylinders. Additional evidence for this coordinated transition can be found in the SAXS data from ISD4 (Figure 6) (and ISD1, Figure 2). The transition from lamellae to cylinders produces two effects. First, there is a change in the relative spacing of the diffraction peaks from q^*, $2q^*$ to q^*, $\sqrt{3}q^*$. Second, a broad maximum appears that spans most of the experimental q range. This second effect is attributed to coil scattering from within the S + I mixed domain, corroborating our two-domain phase assignment. It persists into the disordered state (Figures 3 and 6) where it is better described as a three-block correlation hole effect. (In a separate publication,[37] we report an extension of the two block RPA theory to ABC triblock copolymers.)

In addition to these morphological differences, the ISD and SID block copolymers display rather different ODT temperatures. ISD1 and SID7 were designed for this comparison. Even though the molecular weight of ISD1 is slightly higher than SID7 its T_{ODT} is 110 °C lower. This result also is consistent with the χ arguments. Contrary to the situation with SID, where there are no direct S/D contacts in the ordered state, disordering offers ISD the best opportunity to minimize such interactions. As a consequence, order is lost at a significantly lower temperature in the former. (This effect also is captured by the RPA calculation.[37])

Binary Triblock Blends. Our interpretation of the neat triblock phase behavior provides the basis for understanding the blend results illustrated in Figure 11. First, we deal with the addition of small amounts of SID to the two-domain cylindrical ISD phase. Because this enhances I/D at the expense of S/D contacts, this should further stabilize the mixed I + S domain as sketched in Figure 12. Conversely, adding a little ISD to the three-domain lamellae SID morphology creates a packing problem. Either complete phase separation or some form of frustrated mixing will occur. Our data indicate a state of mixing is achieved, with retention of the three-domain lamellae morphology with up to 15% ISD at 70 °C (see Figures 9 and 11). Figure 12 illustrates the most likely scheme for accommodating such a

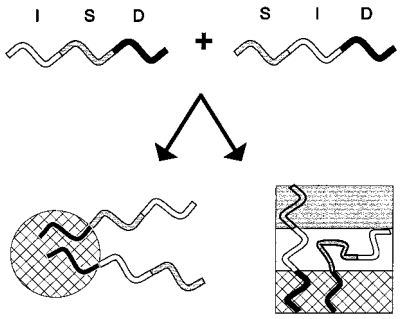

Figure 12. Schematic arrangement of ISD and SID molecules in blended samples. In cylindrical and gyroid morphologies, channels of D are surrounded by a matrix of mixed S and I. In the lamellar state, ISD "folds" into the three-domain SID microstructure.

mixture, where the S and I blocks in the minority ISD component mix with the I blocks from the majority SID compound. Increased amounts of ISD will strain the lamellae morphology due to the accumulation of I and S blocks (from ISD) within the S domain (see Figure 12), leading to a phase transition. Given the two-domain cylindrical ISD structure S + I domain mixing seems like the most logical mechanism for relieving this packing dilemma.

Perhaps the most interesting aspect of this blend study is the occurrence of the gyroid morphology over a relatively wide range of compositions in the center of the phase diagram (Figure 11). This structure is well established in theory[3] and practice[41] for AB diblock and ABA triblock copolymers, located within 3−4% composition windows near the ODT on either side of the phase diagram. Figure 11 bears certain similarities to this documented behavior: The G window is located between cylindrical and lamellae phases, and borders the disordered state, and it occurs at a psuedocomposition of approximately $^2/_3$ volume fraction assuming a mixed S + I domain. However, we have induced the formation of the G phase by blending equal composition triblocks, neither of which displays this phase in the neat form, rather than through the conventional manipulation of composition. While there is a precedence for blending lamellae and cylinder forming diblocks to generate the G phase,[27] to the best of our knowledge this has not been accomplished at constant composition.

What then controls the transition from cylinders to gyroid (and then to lamellae) as SID is added to ISD? We speculate that a changing interfacial tension is responsible. Notwithstanding S + I mixing the composition adjacent to the D interface must be richer in segments associated with the block connected to the D block. Thus, as SID is added to ISD, the interfacial composition will shift toward I. As a consequence, the interfacial tension (i.e., the effective χ parameter) will decrease. Block copolymer phase behavior is established through a balance between interfacial free energy and chain stretching.[16] The substantial difference between χ_{SD} and χ_{ID} (about 34% larger at 130 °C) likely contributes to the documented transition from two-domain cylinders to gyroid at 40−50% SID. Conformational effects also may contribute to this effect, although the cylinders and gyroid phases share a similar mixed S + I state. This line of reasoning is less easily extended to the lamellae morphology where packing frustration is created by the three-domain arrangement (see Figure 12).

These findings provide fresh insights into the mechanisms responsible for phase formation in block copolymer melts and suggest new approaches for obtaining specific morphologies subject to compositional constraints. An important extension of this work currently under investigation is stronger segregation where the G phase is extinguished in diblock copolymers. On the basis of the two-domain cylinder to three-domain lamellae transition documented with ISD, we anticipate loss of the G phase as the S + I mixed domain region disappears. This may lead to macroscopic phase separation or a different state of order.

V. Summary

Differences between compositionally symmetric SID and ISD triblock copolymers have been found in the relative ordered-state stability, pathway to disorder, ordered-state symmetry, and disordered-state scattering. Because of the drive to eliminate unfavorable S−D interactions, ISD disorders at a lower temperature than does SID at comparable compositions and molecular weights. With heating, lamellar ISD undergoes a mixing of S and I blocks to dilute S−D interactions. This mixing promotes a transition from a three-domain lamellar to a two-domain cylindrical morphology. Heating SID results in a transition to disorder directly from the lamellar state.

Blends of ISD and SID copolymers having approximately equal segment volume fractions and molecular weights can be alloyed, with gyroid formation over an extensive composition range. As the weight percent of SID increases, the ordered-state morphology evolves from cylindrical, to gyroid, to lamellar. Relative strengths of interaction parameters lead us to deduce that blend self-assembly occurs through mixing of S and I blocks and microphase separation of D blocks.

Acknowledgment. Support for this research was provided by a 3M Fellowship (C.M.H.) and the NSF through Grant NSF/DMR 9905008. The research at Oak Ridge was supported by the Laboratory Directed Research and Development Program of Oak Ridge National Laboratory, and by the Division of Materials Sciences, under Contract DE-AC05-00OR22725 with the Oak Ridge National Laboratory, managed by UT-Battelle, LLC. G.D.W. thanks Professor D. Richter for the hospitality of the Forschungszentrum and the assistance provided by the staff of the Institut für Festkörperforschung. We also thank Dr. Dietmer Schwahn for valuable assistance with the SANS experiments and David Morse for enlightening discussions and assistance with the Appendix.

Appendix

Scattering calculations used to generate the solid lines in Figure 2 are described in detail elsewhere.[42] Estimated Bragg reflection intensities for each permissible wavevector **G** modify the amplitudes of Dirac delta functions that represent scattering from a perfect lattice having the specified crystalline symmetry:

$$I(q) = \sum_G A_G \delta(q - G) \tag{1}$$

The integrated scattering intensity magnitude A_G for each allowed wavevector G is proportional to the square modulus of the Fourier transform of the electron density

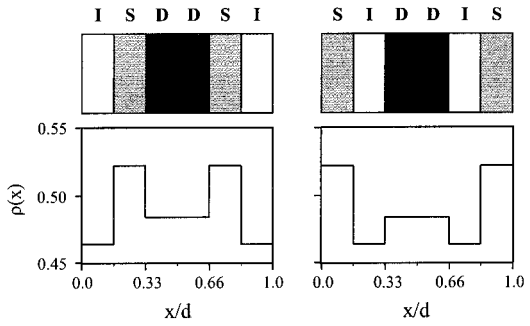

Figure 13. Idealized electron density profiles used in predicting the change in relative peak intensities between lamellar ISD and SID. Molar electron densities for S, I, and D blocks were approximated as 0.522, 0.464, and 0.484 mol/cm^3, respectively. Above are the plots for a sample with perfectly symmetric compositions; experimentally deduced volume fractions were used in the plotted calculations. Shuffling the order of microdomains causes the changes in experimental and calculated relative peak intensities shown in Figure 2.

profile over a unit cell,

$$A_G \propto |\tilde{\rho}(G)|^2 \tag{2}$$

where

$$\tilde{\rho}(G) = \int_{\text{cell}} \rho(\mathbf{r}) e^{-i\mathbf{G}\cdot\mathbf{r}}\, d\mathbf{r} \tag{3}$$

The local electron density ρ at a position $\mathbf{r}$ is calculated from published homopolymer mass densities.

For lamellar morphologies, electron densities deduced from the mass densities of each block were used to construct an electron density profile having three distinct microdomains as shown in Figure 13.

Calculations for hexagonally packed cylindrical morphologies were considered for both the case of homogeneous cylinders (constant density) and for core−shell cylinders (one step change in $\rho(r)$ within the cylinder; see Figure 2). For $G \neq 0$, $\tilde{\rho}(G)$ is unchanged when $\rho(r)$ is shifted by a constant. We take advantage of this in the calculation for the hexagonal phase by subtracting the matrix density from the cylindrical shell and core densities. This step eliminates having to compute an integral over a hexagonal region. We carry out angular integrals in the hexagonal phase using[43]

$$J_0(z) = \frac{1}{\pi}\int_0^{\pi} e^{iz\cos\theta}\, d\theta \tag{4}$$

and carry out the remaining integral numerically. In all cases the location of the first-order reflection was fixed according to the SAXS data.

References and Notes

(1) Fredrickson, G. H.; Bates, F. S. *Annu. Rev. Mater. Sci.* **1996**, *26*, 501.
(2) Khandpur, A. K.; Förster, S.; Bates, F. S.; Hamley, I. W.; Ryan, A.; Bras, W.; Almdal, K.; Mortensen, K. *Macromolecules* **1995**, *28*, 8796.
(3) Matsen, M. W.; Bates, F. S. *Macromolecules* **1996**, *29*, 1091.
(4) Leibler, L. *Macromolecules* **1980**, *13*, 1602.
(5) Matsushita, Y.; Choshi, H.; Fujimoto, T.; Nagasawa, M. *Macromolecules* **1980**, *13*, 1053.
(6) Matsushita, Y.; Yamada, K.; Hattori, T.; Fujimoto, T.; Sawada, Y.; Nagasawa, M.; Matsui, C. *Macromolecules* **1983**, *16*, 10.
(7) Auschra, C.; Stadler, R. *Macromolecules* **1993**, *26*, 6364.
(8) Auschra, C.; Stadler, R. *Macromolecules* **1993**, *26*, 2171.
(9) Krappe, U.; Stadler, R.; Voigt-Martin, I. *Macromolecules* **1995**, *28*, 4458.
(10) Stadler, R.; Aschura, C.; Beckmann, J.; Krappe, U.; Voigt-Martin, I.; Leibler, L. *Macromolecules* **1995**, *28*, 3080.
(11) Shefelbine, T. A.; Vigild, M. E.; Matsen, M. W.; Hajduk, D. A.; Hillmyer, M. A.; Cussler, E. L.; Bates, F. S. *J. Am. Chem. Soc.* **1999**, *121*, 8457.
(12) Zheng, W.; Wang, Z. G. *Macromolecules* **1995**, *28*, 7215.
(13) Bohbot-Raviv, Y.; Wang, Z. G. *Phys. Rev. Lett.* **2000** *85*, 3428.
(14) Beckmann, J.; Auschra, C.; Stadler, R. *Macromol. Rapid Commun.* **1994**, *15*, 67.
(15) Breiner, U.; Krappe, U.; Thomas, E.; Stadler, R. *Macromolecules* **1998**, *31*, 135.
(16) Bates, F. S.; Fredrickson, G. H. *Phys. Today* **1999**, *52*, 32.
(17) Matsen, M. W.; Schick, M. *Phys. Rev. Lett.* **1994**, *72*, 2660; *Macromolecules* **1994**, *27*, 6761; *Macromolecules* **1994**, *27*, 7157.
(18) Drolet, F.; Fredrickson, *Phys. Rev. Lett.* **1999**, *83*, 4317.
(19) Bates, F. S.; Schulz, M. F.; Khandpur, A. K.; Förster, S. Rosedale, J. H.; Almdal, K.; Mortensen, K. *Faraday Discuss.* **1994**, *98*, 7.
(20) Sugiyama, M.; Shefelbine, T. A.; Vigild, M. E.; Bates, F. S., submitted to *J. Phys. Chem. B.*
(21) Ndoni, S.; Papadakis, C. M.; Bates, F. S.; Amdal, K. *Rev. Sci. Instrum.* **1995**, *66*, 1090.
(22) Lodge, T. P.; Pan, C.; Jin, X.; Liu, Z.; Zhao, J.; Maurer, W. W.; Bates, F. S. *J. Polym. Sci., Polym. Phys. Ed.* **1995**, *33*, 2289.
(23) Hajduk, D. A.; Takenouchi, H.; Hillmyer, M. A.; Bates, F. S.; Vigild, M. E.; Almdal, K. *Macromolecules* **1997**, *30*, 3788.
(24) Lipic, P. M.; Bates, F. S.; Matsen, M. W. *J. Polym. Sci., Part B* **1999**, *37*, 2229.
(25) Abetz, V.; Stadler, R. *Macromol. Symp.* **1997**, *113*, 19.
(26) Hueckstaedt, H.; Goepfert, A.; Abetz, V. *Polymer* **2000**, *41*, 9089.
(27) Zhao, J.; Majumdar, B.; Schulz, M. F.; Bates, F. S.; Almdal, K.; Mortensen, K.; Hajduk, D. A.; Gruner, S. M. *Macromolecules* **1996**, *29*, 1204.
(28) Abetz, V.; Goldacker, T. *Macromol. Rapid Commun.* **2000**, *21*, 16.
(29) Ndoni, S.; Papdakis, C. M.; Bates, F. S.; Amdal, K. *Rev. Sci. Instrum.* **1995**, *66*, 1090.
(30) Maschke, U.; Wagner, T.; Coqueret, X. *Mackromol. Chem.* **1992**, *193*, 2543.
(31) Fetters, L. J.; Lohse, D. J.; Richter, D.; Witten, T. A.; Zirkel, A. *Macromolecules* **1994**, *27*, 4639.
(32) *Neutronenstreuexperimente am FRJ2 in Jülich*, 1997 (English and German texts are available from the Forschungszentrum, Jülich).
(33) Wignall, G. D.; Christen, D. K.; Ramakrishnan, V. *J. Appl. Crystallogr.* **1988**, *21*, 438.
(34) Rosedale, J. H.; Bates, F. S. *Macromolecules* **1990**, *23*, 2329.
(35) Widmaier, J. M.; Meyer, G. C. *J. Polym. Sci., Polym. Phys. Ed.* **1980**, *18*, 2217.
(36) Han, C. D.; Kim, J. *J. Polym. Sci., Polym. Phys. Ed.* **1987**, *25*, 1741.
(37) Cochran, E. W.; Morse, D. A.; Bates, F. S. Manuscript in preparation.
(38) Hamley, I. W.; Koppi, K. A.; Rosedale, J. H.; Bates, F. S.; Amdal, K.; Mortensen, K. *Macromolecules* **1993**, *26*, 5959.
(39) Hajduk, D. A.; Gruner, S. M.; Rangarajan, P.; Register, R. A.; Fetters, L. J.; Honeker, C. C.; Albalak, R. J.; Thomas, E. L. *Macromolecules* **1994**, *27*, 4063.
(40) Kossuth, M. B.; Morse, D. C.; Bates, F. S. *J. Rheol.* **1999**, *43*, 167.
(41) Avgeropoulos, A.; Dair, B. J.; Hadjichristidis, N.; Thomas, E. L. *Macromolecules* **1997**, *30*, 5634.
(42) Higgins, J. S.; Benoît, H. C. *Polymers and Neutron Scattering*; Oxford University Press: New York, 1994. Honeker, C. Ph.D. Thesis, Massachusetts Institute of Technology, 1997.
(43) Oliver, F. W. J. In *Handbook of Mathematical Functions*; Abramowitz, M., Stegun, I. A., Eds.; Dover Publications: New York, 1970; p 360.

MA0115489